Strong magnetochiral dichroism of helical structures of garnet particles

Aristi Christofi* and Nikolaos Stefanou

University of Athens, Department of Solid State Physics, Panepistimioupolis, GR-157 84 Athens, Greece
**Corresponding author: aristi@ims.demokritos.gr*

Received September 4, 2013; revised October 2, 2013; accepted October 7, 2013;
posted October 7, 2013 (Doc. ID 197017); published November 6, 2013

We report on the occurrence of strong nonreciprocal magnetochiral dichroism in helical structures of magnetic garnet spheres, which emerges as a result of the simultaneous lack of time-reversal and space-inversion symmetries, by means of rigorous full-electrodynamic calculations using the layer-multiple-scattering method. It is shown that a strong effect appears in flat band regions associated with enhanced natural and magnetic optical activity. © 2013 Optical Society of America

OCIS codes: (050.1930) Dichroism; (050.5298) Photonic crystals; (160.1585) Chiral media; (160.3820) Magneto-optical materials; (230.2240) Faraday effect.
http://dx.doi.org/10.1364/OL.38.004629

A static magnetic field parallel to the direction of propagation of an incident light beam can produce a small shift in the value of the permittivity of a chiral structure or substance. This shift is independent of the polarization characteristics of the light beam and changes sign either on replacing the chiral structure/substance by its mirror-image enantiomer or on reversing the relative directions of the magnetic field and propagation of the light beam. As a result, so-called magnetochiral, anisotropy effects have long been anticipated theoretically, either in refraction (birefringence) or in absorption/emission (dichroism) [1–7]. It should be emphasized that these effects are clearly nonreciprocal, arising from the simultaneous lack of time-reversal and space-inversion symmetries in a material that possesses magnetic moment and spatial asymmetry and should be distinguished from their reciprocal counterparts, which are induced solely by either the chiral structure or the magnetic field. Magnetochiral anisotropy, besides being interesting as such since it relates to fundamental symmetry principles that govern light–matter interaction, has also been proposed as a possible explanation for the homochirality of life, because it enables enantioselective photochemistry in a magnetic field with unpolarized light [8]. Magnetochiral birefringence and dichroism, as second-order cross effects, are generally rather weak and, therefore, well-prepared experiments on carefully selected systems are required for their unambiguous observation. So far, experimental evidence for these effects has been reported on liquid molecular systems, organic compounds, chiral uniaxial crystalline materials, and chiral ferromagnets [8–16]. Recently, possible configurations where such direction-dependent optical phenomena can emerge were determined using symmetry considerations, and the design of tailored magnetic metamaterials and photonic crystals that would largely extend the applicability of these phenomena was anticipated [17].

In this Letter, we propose a photonic crystal consisting of magnetic garnet particles in a helical arrangement, embedded in a low-refractive-index nonmagnetic dielectric host material, as a versatile structure that exhibits strong magnetochiral dichroism. Magnetic garnet particles can be synthesized in the laboratory [18–20] and assembled into helical structures using, e.g., directed assembly techniques, while the spectral response of the photonic crystal can be tuned within the visible and infrared range by appropriately choosing the geometric parameters involved.

At visible and infrared frequencies, the gyrotropic response of materials is rather weak and can be described by a (relative) magnetic permeability $\mu_g = 1$ and (relative) electric permittivity tensor of the form

$$\overleftrightarrow{\epsilon_g} = \epsilon_r \begin{pmatrix} 1 & -ig & 0 \\ ig & 1 & 0 \\ 0 & 0 & 1 \end{pmatrix}, \tag{1}$$

if the gyration vector is oriented along the z direction. In the present work we assume $\epsilon_r = 6.25 + 0.001i$, which is a typical value for a low-loss magnetic garnet material, and gyrotropy parameter $g = 0.01$, which is achievable with magnetic garnets [21–23]. We consider a tetragonal crystal defined by the primitive lattice vectors $\mathbf{a}_1 = (a, 0, 0)$, $\mathbf{a}_2 = (0, a, 0)$, $\mathbf{a}_3 = (0, 0, c)$ and a basis of four magnetic garnet spheres, of radius S, centered at (0,0,0), $(b, 0, c/4)$, $(b, b, c/2)$, and $(0, b, 3c/4)$, as shown in Fig. 1, embedded in a homogeneous host medium of relative electric permittivity $\epsilon = 1$ and magnetic permeability $\mu = 1$. This chiral structure with nonmagnetic dielectric spheres was originally proposed as an artificial strongly optically active material [24]. Here we take $c/a = 2$, $b/a = 0.25$, and $S/a = 0.25$ and calculate the optical properties of this crystal by the layer-multiple-scattering method [25,26], properly extended to the case of gyrotropic spherical scatterers [27].

To begin with, we summarize the main features of the photonic band structure of the crystal under consideration with unmagnetized garnet spheres [$g = 0$ in Eq. (1)], neglecting dissipative losses in order to ensure an unambiguous interpretation of the calculated dispersion diagram. As shown in Fig. 1, along the [001] direction, at low frequencies (below $\omega a/2\pi c_0 \cong 0.7$) we obtain two nondegenerate extended bands folded within the first Brillouin zone so close to each other that they are indistinguishable at the scale of the figure, associated with propagation in a homogeneous effective medium.

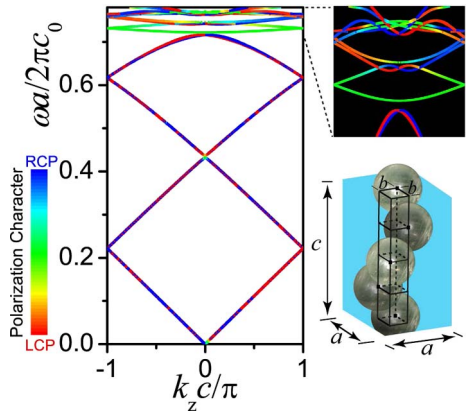

Fig. 1. Photonic band structure along the [001] direction of a tetragonal crystal with a basis of four unmagnetized lossless garnet spheres, of radius S, in a helical arrangement in the unit cell as shown in the margin ($c/a = 2$, $b/a = 0.25$, $S/a = 0.25$). An enlarged view of the dispersion diagram in the region of the narrow bands is also displayed.

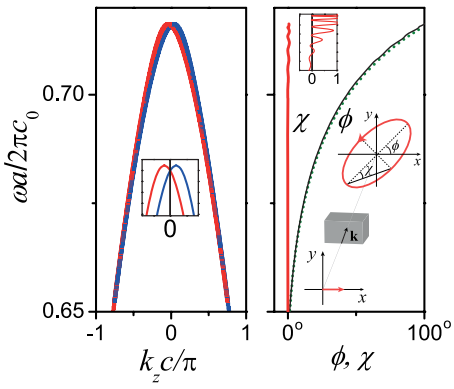

Fig. 2. Left-hand diagram: An enlarged view of the dispersion diagram of Fig. 1 below the gap that separates the extended from the flat bands. Right-hand diagram: Ellipticity and azimuth rotation angles of the transmitted wave for light linearly polarized along the x axis, incident normally on a (001) slab of the crystal consisting of 64 layers of spheres, including dissipative losses. The azimuth rotation angle is calculated from the dispersion diagram (dotted line) and directly obtained from the transmitted wave (solid lines).

At higher frequencies, the dispersion diagram is characterized by the presence of additional narrow bands, which stem from weakly interacting Mie resonant modes of the individual spheres at $\omega a/2\pi c_0 = 0.76$ (magnetic dipole mode), $\omega a/2\pi c_0 = 0.91$ (electric dipole mode), $\omega a/2\pi c_0 = 1.09$ (magnetic quadrupole mode), etc. Anticrossing interaction between narrow and extended bands gives rise to the formation of frequency gaps and hybridized bands that have strong admixture of the localized resonant modes in their flat parts like, e.g., at the top of the bands below the small gap at $\omega a/2\pi c_0 = 0.72$ (see the enlarged view of the dispersion diagram in the margin of Fig. 1). It is worth noting that, though this crystal does not possess space-inversion symmetry, the symmetry $\omega(-\mathbf{k}) = \omega(\mathbf{k})$ persists because of time-reversal symmetry. Group theory dictates that the bands along the given direction are nondegenerate and none of them corresponds to purely left- or right-circularly polarized (LCP and RCP, respectively) Bloch modes [27]. There is a different degree of LCP and RCP admixture that varies continuously along a specific band, as presented by the color scale in Fig. 1 that shows the projection of the corresponding eigenvectors (Bloch modes) onto the basis spanned by the LCP and RCP states.

Up to $\omega a/2\pi c_0 = 0.72$, at each frequency we obtain two modes, one of LCP and one of RCP predominant character, propagating in the forward (positive z) direction and two corresponding backward propagating modes. Therefore, a linearly polarized electromagnetic wave of angular frequency ω in this spectral region, incident normally on a finite (001) slab of the crystal, is decomposed into an LCP and an RCP wave, which propagate through the slab with different phase velocities: ω/k_z^L and ω/k_z^R, respectively, where $k_z^R - k_z^L \equiv \Delta k_z$ is the band splitting at the given frequency. If the LCP and RCP components of the transmitted wave have the same amplitude, the transmitted wave will be linearly polarized with a polarization direction at an angle $\phi = \Delta k_z d/2$ relative to the polarization direction of the incident wave (optical activity), where d is the thickness of the slab and a positive ϕ means an anticlockwise rotation. In general, the transmitted wave is elliptically polarized with the long axis of the ellipse forming an angle $\phi = [\arg(E_{\mathrm{tr}}^R) - \arg(E_{\mathrm{tr}}^L)]/2$ with the polarization direction of the incident wave and with ellipticity angle $\chi = \arctan[(|E_{\mathrm{tr}}^R| - |E_{\mathrm{tr}}^L|)/(|E_{\mathrm{tr}}^R| + |E_{\mathrm{tr}}^L|)]$, where E_{tr}^R, E_{tr}^L are the complex electric field amplitudes of the RCP and LCP components of the transmitted wave.

As can be seen in the right-hand diagram of Fig. 2, the ellipticity angle is vanishingly small and near the top of the bands exhibits small oscillations. We note that a linearly polarized transmitted wave is obtained if $\chi = 0$. In the same diagram, we also display the variation of ϕ, as calculated from both the dispersion diagram of the infinite crystal and the transmitted wave through the given finite slab. The results obtained by the two methods are in excellent agreement, which shows that the bulk behavior where ϕ varies linearly with the slab thickness is attained [28]. It can be seen that the optical activity increases as we approach the flat region at the top of the bands, where they have a large splitting Δk_z (band-edge effect).

If the garnet spheres are magnetized along the z direction, spectral nonreciprocity $\omega(-\mathbf{k}) \neq \omega(\mathbf{k})$ is clearly manifested as a result of time-reversal symmetry breaking in conjunction with the lack of space-inversion symmetry [29], as can be seen in the band diagram of Fig. 3. In the forward direction, the optical activity induced by the helical structure partly counterbalances the magnetic optical activity (Faraday rotation) while in the backward direction chirality and magnetism contribute constructively to yield a strongly enhanced polarization azimuth rotation.

Because of the pronounced natural, i.e., chirality induced, and magnetic optical activity exhibited by the given crystal, we also expect strong magnetochiral anisotropy effects, e.g., in optical absorption, in the frequency region under consideration. As a quantitative measure of magnetochiral dichroism, we adopt the normalized anisotropy factor $\Delta\mathcal{A}/\langle\mathcal{A}\rangle$ [10], with $\Delta\mathcal{A} \equiv$

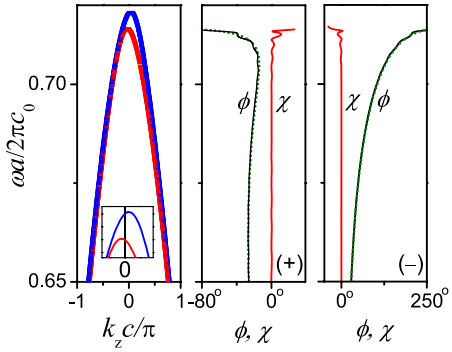

Fig. 3. Same as in Fig. 2 for garnet spheres magnetized along the z direction. The corresponding variations of the ellipticity and azimuth rotation angles are displayed for both forward (+) and backward (−) transmitted waves.

$\mathcal{A}_+ - \mathcal{A}_-$ and $\langle\mathcal{A}\rangle \equiv (\mathcal{A}_+ + \mathcal{A}_-)/2$ where $\mathcal{A}_{+(-)}$ is the absorbance of unpolarized light incident on a slab of the crystal in (opposite to) the direction of magnetization of the garnet spheres. We note in passing that unpolarized light can be regarded as an incoherent superposition of LCP and RCP, or in general of any two orthonormal polarization, light modes. As can be seen in Fig. 4, strong magnetochiral dichroism, which corresponds to values of the normalized anisotropy factor as large as 0.1, is obtained near the top of the bands of Fig. 3 where enhanced natural and magnetic optical activity is encountered. The absorption difference, $\Delta\mathcal{A}$, increases with the slab thickness, but so does the (average) absorption, $\langle\mathcal{A}\rangle$, so that the optimal magnetochiral dichroism anisotropy factor, $\Delta\mathcal{A}/\langle\mathcal{A}\rangle$, is obtained for slabs of moderate thickness, for example a slab 64-layers thick.

In summary, we proposed and analyzed, based on rigorous full-electrodynamic calculations by the layer-multiple-scattering method, a photonic crystal of magnetic garnet spheres in a helical arrangement that exhibits strong magnetochiral dichroism, which exceeds by at least one-order of magnitude that found in naturally occurring media. This behavior is related to the concurrent large natural and magnetic optical activity that the crystal exhibits in certain frequency regions, which can be tuned within the visible and infrared spectrum by appropriately selecting the geometric parameters involved. We note that, using spheres with a different magneto-optical response, the effect changes accordingly. For example, if $g = 0.005$, smaller values of $\Delta\mathcal{A}/\langle\mathcal{A}\rangle$ that do not exceed 0.05 are obtained. On the other hand, structure optimization can lead to an enhanced effect. Therefore our study, besides its fundamental interest, paves the way to the design of artificial nanostructures with stronger magneto-chiral anisotropy, which may find practical applications in miniaturized nonreciprocal photonic devices.

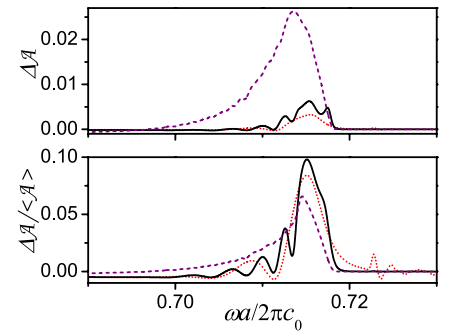

Fig. 4. Magnetochiral dichroism of (001) slabs of the crystal of magnetic garnet spheres under consideration, at normal incidence, near the top of the bands of Fig. 3. Dotted lines: 32 layers thick slab. Solid lines: 64 layers thick slab. Dashed lines: 1024 layers thick slab.

Aristi Christofi is supported by a SPIE Optics and Photonics Education Scholarship.

References

1. M. P. Groenewege, Mol. Phys. **5**, 541 (1962).
2. W. F. Brown, Jr., S. Shtrieman, and D. Treves, J. Appl. Phys. **34**, 1233 (1963).
3. D. L. Portigal and E. Burstein, J. Phys. Chem. Solids **32**, 603 (1971).
4. N. B. Baranova, Yu. V. Bogdanov, and B. Ya. Zel'Dovich, Opt. Commun. **22**, 243 (1977).
5. N. B. Baranova and B. Ya. Zel'Dovich, Mol. Phys. **38**, 1085 (1979).
6. G. Wagnière and A. Meier, Chem. Phys. Lett. **93**, 78 (1982).
7. L. D. Barron and J. Vrbancich, Mol. Phys. **51**, 715 (1984).
8. G. L. J. A. Rikken and E. Raupach, Nature (London) **405**, 932 (2000).
9. G. L. J. A. Rikken and E. Raupach, Nature (London) **390**, 493 (1997).
10. G. L. J. A. Rikken and E. Raupach, Phys. Rev. E **58**, 5081 (1998).
11. P. Kleindienst and G. H. Wagnière, Chem. Phys. Lett. **288**, 89 (1998).
12. N. K. Kalugin, P. Kleindienst, and G. H. Wagnière, Chem. Phys. **248**, 105 (1999).
13. M. Vallet, R. Ghosh, A. Le Floch, T. Ruchon, F. Bretenaker, and J.-Y. Thepot, Phys. Rev. Lett. **87**, 183003 (2001).
14. C. Train, R. Gheorghe, V. Krstic, L.-M. Chamoreau, N. S. Ovanesyan, G. L. J. A. Rikken, M. Gruselle, and M. Verdaguer, Nat. Mater. **7**, 729 (2008).
15. Y. Kitagawa, H. Segawa, and K. Ishii, Angew. Chem. Int. Ed. **50**, 9133 (2011).
16. Y. Kitagawa, T. Miyatake, and K. Ishii, Chem. Commun. **48**, 5091 (2012).
17. D. Szaller, S. Bordács, and I. Kézsmárki, Phys. Rev. B **87**, 014421 (2013).
18. N. Yahya, R. M. Al Habashi, K. Koziol, R. D. Borkowski, M. N. Akhtar, M. Kashif, and M. Hashim, J. Nanosci. Nanotechnol. **11**, 2652 (2011).
19. D. T. T. Nguyet, N. P. Duong, T. Satoh, L. N. Anh, and T. D. Hien, J. Alloys Comp. **541**, 18 (2012).
20. R. J. Ji, W. Yin, C. Fang, and Y. Zeng, J. Mater. Chem. C **1**, 1763 (2013).
21. S. M. Drezdzon and T. Yoshie, Opt. Express **17**, 9276 (2009).
22. A. B. Khanikaev, S. H. Mousavi, G. Shvets, and Y. S. Kivshar, Phys. Rev. Lett. **105**, 126804 (2010).
23. K. Fang, Z. Yu, V. Liu, and S. Fan, Opt. Lett. **36**, 4254 (2011).
24. V. Karathanos, N. Stefanou, and A. Modinos, J. Mod. Opt. **42**, 619 (1995).
25. N. Stefanou, V. Yannopapas, and A. Modinos, Comput. Phys. Commun. **113**, 49 (1998).
26. N. Stefanou, V. Yannopapas, and A. Modinos, Comput. Phys. Commun. **132**, 189 (2000).
27. A. Christofi and N. Stefanou, Phys. Rev. B **87**, 115125 (2013).
28. A. B. Khanikaev, A. B. Baryshev, P. B. Lim, H. Uchida, M. Inoue, A. G. Zhdanov, A. A. Fedyanin, A. I. Maydykovskiy, and O. A. Aktsipetrov, Phys. Rev. B. **78**, 193102 (2008).
29. A. Figotin and I. Vitebsky, Phys. Rev. E **63**, 066609 (2001).